# ATBD

Algorithm Theoretical Base Document

## MapBiomas Chile

Glaciers — Collection 1

**General Coordinator:**
Jaime Hernández

**Technical Coordinator:**
Eliana Fonseca

**Team Chile**
Carlos Hormazábal, Alberto Cisternas, Sophía Barría, Valeria Castro, Diego Muñoz y Rodrigo Fuentes

*July 2026*

**TABLE OF CONTENTS**

# 1 Introduction

## 1.1 Scope and Content

This Algorithm Theoretical Base Document (ATBD) describes the methodology used to produce the annual glacier surface area dataset for Chile as part of MapBiomas Agua Chile Collection 1. The dataset provides a consistent 28-year time series (1998–2025) of bare-ice glacier extent at 30 m spatial resolution, mapped annually across the four Chilean glaciological macrozones: Norte, Centro, Sur, and Austral.

## 1.2 Methodological Overview

The methodology combines multitemporal satellite image compositing, supervised Random Forest classification, gap-filling, and temporal post-processing to discriminate bare-ice glaciers from snow, rock, and other land surface types. Temporal filters applied after classification enforce physical consistency across the time series — ensuring that detected glacier gains and losses reflect real cryospheric dynamics rather than interannual classification noise associated with seasonal snow or cloud contamination.

## 1.3 Region of Interest

The mapping covers continental Chile (approximately 17.5°S to 56°S), subdivided into four glaciological macrozones following the classification of the Dirección General de Aguas (DGA). The following characterization of each macrozone is based on DGA (2011):

- **North Macrozone (~17.5°–32°S):** Arid, high-elevation Andes. Glaciers and glacierets are scarce and predominantly small, mostly above 4,500 m a.s.l.; many are cold-based bodies that lose mass chiefly through sublimation rather than melt, and rock glaciers are abundant.

- **Center Macrozone (~32°–36°S):** Temperate mountain and valley glaciers under a Mediterranean, winter-dominated precipitation regime. Frequently debris-covered and hydrologically significant, as glacier melt sustains a substantial share of river flow during dry periods in the basins serving central Chile.

- **South Macrozone (~36°–46°S):** Mountain and valley glaciers transitioning toward the Patagonian regime, largely concentrated on Andean stratovolcanoes, under an increasingly humid maritime climate. Ice extent has undergone marked area loss in recent decades.

- **Austral Macrozone (~46°–56°S):** Patagonian icefields and their outlet glaciers, including the Northern and Southern Patagonian Icefields and the Cordillera Darwin, with numerous tidewater/calving glaciers under a maritime, hyperhumid climate. Frontal retreat and area loss are generalized across the zone, with a small number of glaciers advancing in the Chilean sector.

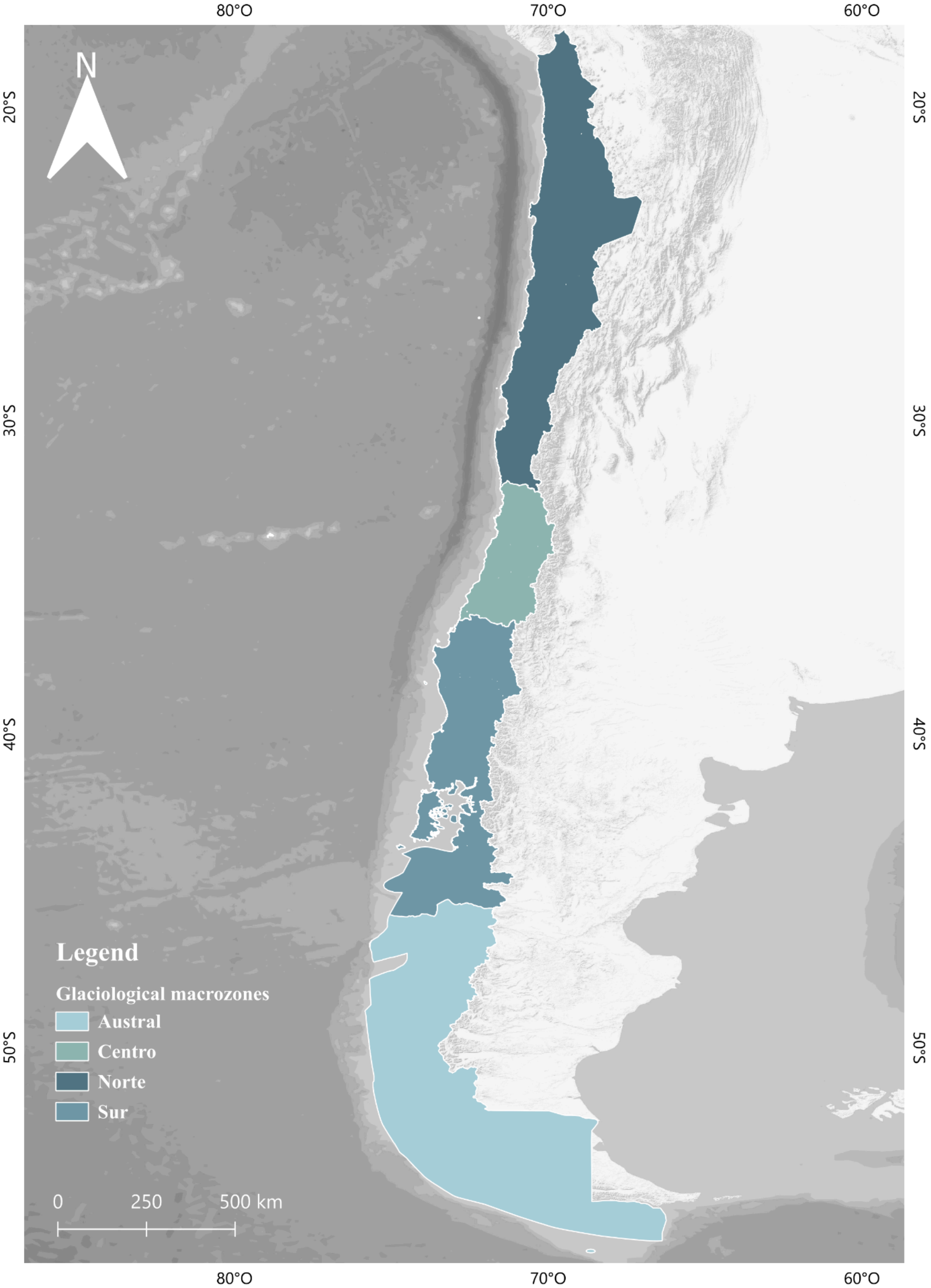


*Figure 1. Glaciological macrozones of Chile.*

## 1.4 Key Applications

The glacier time series supports: long-term monitoring of glacier area change in response to climate variability; assessment of water resource contributions from glacial melt; validation and calibration of glaciological and hydrological models; reporting on national and international cryosphere indicators; and integration with the broader MapBiomas land cover and water surface datasets.

# 2 Background

## 2.1 Context

According to the 2022 Public Glacier Inventory (Inventario Público de Glaciares, IPG 2022; DGA, 2022) continental Chile contains 26,180 glaciers covering 21,012 km² — equivalent to 2.79% of the national territory and approximately 76% of the total glacier area of the Southern Andes. Chilean glaciers span a wide latitudinal and climatic gradient, from small subtropical glacierets in the Dry Andes to large tidewater glaciers in Patagonia. Despite their importance as freshwater reserves and climate indicators, continuous annual monitoring of glacier extent at the national scale has been constrained by data availability and methodological challenges.

Recent studies document accelerating glacier mass loss across the Andes. Dussaillant et al. (2019) reported an Andes-wide mass loss of $-22.9 \pm 5.9$ Gt $yr^{-1}$ between 2000 and 2018, with the Dry and Central Andes shifting from close to balance during 2000–2009 to strongly negative during 2009–2018, coinciding with the Chilean megadrought. Saavedra et al. (2026) documented a spatially coherent decline in snow persistence between 29°S and 36°S from 2000 to 2025, with snowline elevations rising at 5–15 m $yr^{-1}$. These trends provide the climatic context within which the glacier classification time series is interpreted.

## 2.2 Reference Inventory

The IPG 2022 serves as the primary ancillary dataset for this classification. Published in May 2022 as an update of the 2014 inventory, it is the most complete and detailed glacier dataset available for Chile, derived from higher-resolution satellite imagery with a mean acquisition date circa 2017, and it incorporates several hundred ice bodies not detected in the 2014 version. Prior to publication it underwent an external validation process in which scientists, consultants and institutions reviewed and commented on the inventory. In this work it is used to derive the minimum glacier elevation per hydrological basin (applied as a spatial constraint within the temporal filter) and to rescue bodies smaller than 0.01 km² using glacieret boundaries. It is not used as a spatial mask restricting detection, in recognition that glacier extent during the early years of the series (1998–2010) exceeded that at the inventory's reference date owing to documented retreat.

# 3 Algorithm Description

The classification pipeline consists of five main stages: i) image collection and mosaic generation, ii) supervised classification, iii) gap-filling, iv) temporal post-processing, and, v) post-classification spatial filtering. All processing was performed within Google Earth Engine (GEE).

Processing is organized at two spatial levels. Mosaic generation, supervised classification, and gap-filling (Sections 3.1–3.4) are performed independently for each ecoregion (Table 1, Figure 2) — the units in which annual composites are built, training samples are collected, and per-year classifications are produced. Temporal and post-classification spatial processing (Sections 3.5–3.6) are then applied at the macrozone level, after the constituent ecoregion classifications are assembled into their corresponding macrozone.

A single post-processing configuration is shared by the North, Center and South macrozones, whereas the Austral macrozone — comprising the Patagonian ecoregions — is processed with a distinct configuration. This reflects the different glaciological regime of the Patagonian icefields: the minimum-persistence rule (Section 3.5.3) is applied to the North, Center and South macrozones but excluded from the Austral macrozone, where glacier fronts undergo genuine multi-year advance–retreat cycles. Independently of this post-processing distinction, the southern zone — the southern portion of the South macrozone and all of the Austral macrozone — additionally integrates Sentinel-2 imagery at the mosaic stage (Section 3.1.2).

*Table 1. Ecoregions description,*

| ID | Ecorregion |
|---|---|
| EC 1 | Dry Puna and Central Andes (Puna Seca y Andina Central) |
| EC 3 | Andean Steppe (Estepa andina) |
| EC6S1 | North Andes (Andes Norte) |
| EC6S2 | Central Andes (Andes Centro) |
| EC6S5 | South Andes (Andes Sur) |
| EC7 | Patagonian Steppe (Estepa patagónica) |
| EC8 | Subpolar Forest (Bosque subpolar) |
| EC9 | Ice and Rocks (Roca y Hielo) |

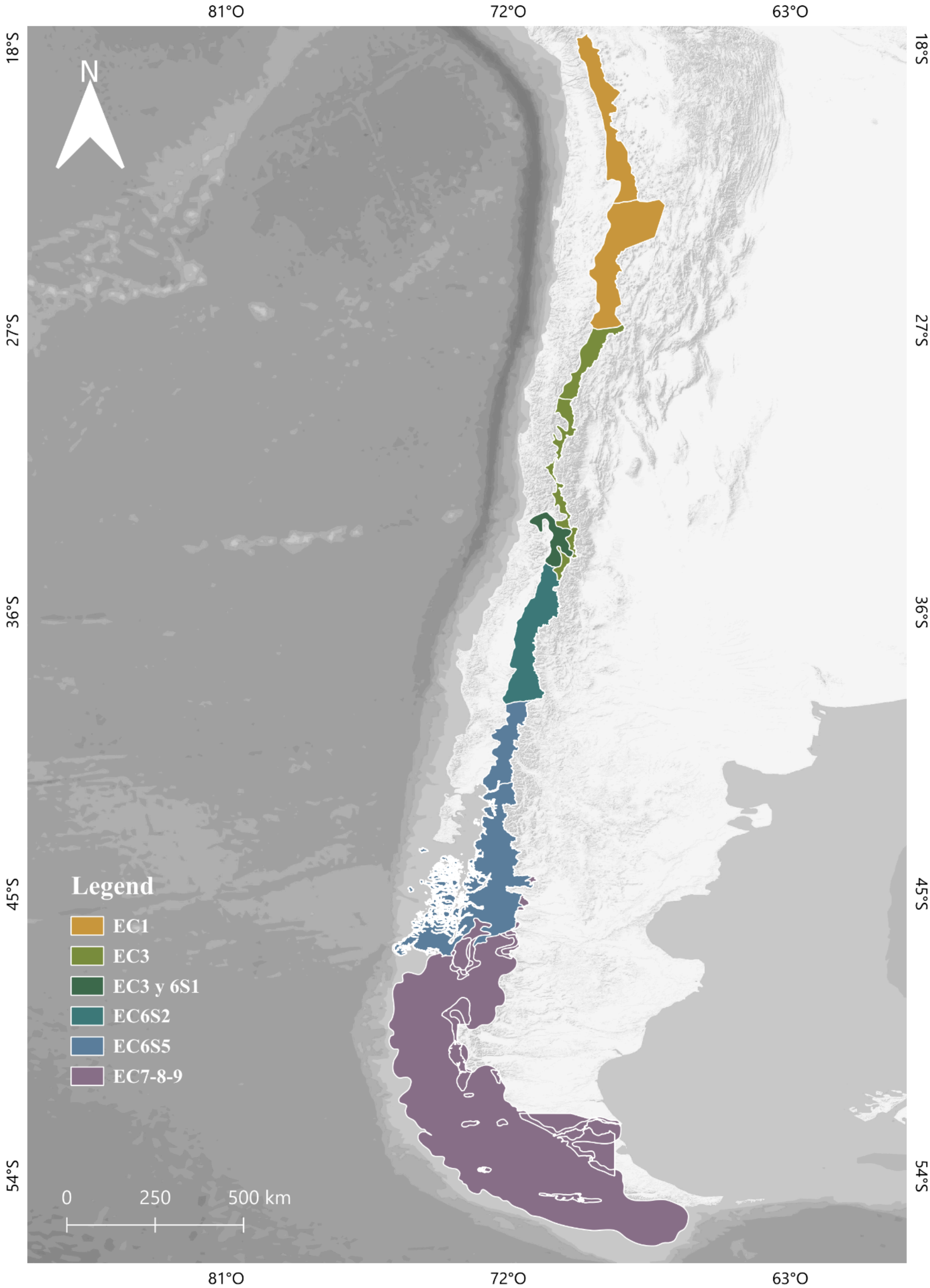


*Figure 2. Ecoregions used as the processing units for mosaic generation and classification.*

## 3.1 Satellite Data

### 3.1.1 Landsat Archive

Annual Top of Atmosphere (TOA) reflectance composites were derived from the Landsat Collection 2 Tier 1 TOA archive (Landsat 5 TM, Landsat 7 ETM+, Landsat 8 OLI, Landsat 9 OLI-2), accessed via GEE. Coverage spans 1998 to 2025 across the full Chilean territory. For each year, images were filtered by acquisition date according to two temporal windows defined by regional precipitation seasonality: November–December for the zone influenced by the Bolivian Winter (altiplano and puna regions of northern Chile), where summer precipitation would otherwise increase snow cover and reduce bare-ice exposure; and December–April for the remainder of the country, capturing late-summer conditions that minimize transient snow cover and maximize bare-ice detection. Cloud and shadow masking was performed using the QA_PIXEL band, which provides pixel-level quality flags including cloud, cloud shadow, snow, and saturation indicators derived from the CFmask algorithm.

### 3.1.2 Southern Zone

South of approximately Puerto Montt (~41.5°S) to the southern tip of the country — a region spanning the southern portion of the South macrozone and the entirety of the Austral macrozone — persistent cloud cover limits the effectiveness of the standard annual Landsat compositing described in Section 3.1.1. A dedicated imagery strategy was therefore applied in this zone, combining manually selected Landsat scenes for the earlier period with Sentinel-2 for the more recent period.

For **1998–2016**, Landsat TOA images were manually selected within a primary temporal window of December–April, consistent with the late-summer compositing strategy applied to the rest of the country. When insufficient usable scenes were available within this window, the selection was extended by one to two months to maximize coverage. Where no adequate imagery could be identified for a given path-row and year, the corresponding area was left as no observation for that year.

For **2017–2025**, Sentinel-2 TOA imagery was incorporated to improve spatial detail and temporal coverage. Cloud masking was performed using the cs_cdf band from Cloud Score+ (GOOGLE/CLOUD_SCORE_PLUS/V1/S2_HARMONIZED; Pasquarella et al., 2023). Both Cloud Score+ bands grade per-pixel usability from 0 (occluded) to 1 (clear); whereas cs scores each observation instantaneously, cs_cdf ranks a pixel's clear-sky score against that same pixel's distribution of scores through time. The cs_cdf band was selected in response to the persistent cloud cover of this zone: because cloud-free acquisitions are scarce, the masking must retain as many usable observations as possible, and cs_cdf masks less aggressively than cs, preserving more usable pixels where clear scenes are limited.

## 3.2 Image Compositing and Mosaic Generation

Annual mosaics were generated at 30 m spatial resolution for each ecoregion tile. The compositing strategy selected low-cloud observations from the late-summer period to generate annual representations of exposed glacier surface. For each year and tile, the following spectral bands and indices were computed and included in the classification feature stack:

- SWIR1 (Short-Wave Infrared 1, ~1.6 μm). useful for discriminating snow/ice from exposed rock, soil, and debris-covered surfaces, as snow and glacier ice show strong absorption in the SWIR region.

- NIR (Near-Infrared, ~0.86 μm): included to capture reflectance differences among snow, ice, vegetation, water, and exposed land surfaces.

- RED (Red, ~0.65 μm): included as a visible reflectance band that provides complementary information on surface brightness and spectral contrast within the classification feature space.

- NDSI (Normalized Difference Snow Index): calculated as (GREEN − SWIR1) / (GREEN + SWIR1); This index was included as a standard spectral indicator of snow and ice, based on their high visible reflectance and low SWIR reflectance.

- ANDSI (Adjusted Normalized Difference Snow Index): calculated following Mohammadi et al. (2023) as (CSI − NDSI) / (CSI + NDSI), where CSI = NIR / SWIR2. ANDSI was included as an additional spectral predictor designed to improve the separability of snow, glacier, and water pixels relative to NDSI alone.

## 3.3 Supervised Classification — Random Forest

Annual glacier extent was mapped using a supervised Random Forest (RF) classifier implemented in GEE. RF was selected for its robustness to class imbalance, capacity to handle correlated features, and reduced sensitivity to overfitting compared to single decision trees.

### 3.3.1 Training Samples

Training samples were collected annually for each ecoregion tile, yielding between 5,000 and 7,000 samples per class. Three classes were sampled: glacier (Class 34), non-glacier (Class 25, encompassing snow, rock, soil, water, and vegetation), and no observation (Class 27). The no observation class was included to handle residual cloud and haze pixels that persisted after the pixel-level quality masking step, allowing the classifier to explicitly identify and exclude contaminated observations rather than propagating them into the annual classification. Sample collection was conducted by visual photo-interpretation of the annual composites directly in GEE, guided by the 2022 Public Glacier Inventory (IPG 2022) as a spatial reference. Samples were distributed to represent the full range of spectral conditions present in each ecoregion and year, including variability in illumination, snow contamination, and glacier surface state.

### 3.3.2 Classification Output

The RF classifier was applied independently for each annual mosaic and ecoregion tile, producing per-pixel annual classifications with three possible values: Class 34 (glacier), Class 25 (non-glacier), and Class 27 (no observation). Class 27 arises from two sources: pixels flagged as no observation by the RF classifier due to residual cloud or haze not removed by the quality masking step, and pixels for which insufficient valid observations were available in the annual compositing window. The initial classification captures bare-ice glacier extent but may include commission errors from persistent seasonal snow, particularly in wet years associated with El Niño events.

## 3.4 Gap-Filling (Step 1)

Pixels classified as no observation (Class 27) — due to residual cloud cover or haze not removed by the quality masking step — were filled using a bidirectional temporal gap-filling procedure. The method fills a no-observation pixel only when consistent evidence exists in both the preceding and following years: if the neighboring years agree on the same class (glacier or non-glacier), the gap is filled with that class; if there is no agreement, the pixel is retained as Class 27. The maximum gap window is 5 years, meaning that a no-observation pixel can be filled by evidence from up to 5 years before or after. For border years (1998 and 2025), where only one temporal neighbor is available, filling is performed using the nearest available observation within a maximum distance of 2 years. This conservative bidirectional approach ensures that gap-filling does not propagate uncertain or inconsistent classifications, and that the resulting time series is spatially as complete as possible without introducing artificial transitions. This step precedes the temporal filter and provides the spatially complete annual stack required for subsequent post-processing.

## 3.5 Temporal Post-Processing (Step 2)

The temporal post-processing stage enforces physical consistency across the annual time series using two complementary filters: an asymmetric temporal filter and a minimum persistence rule (Regla C). Both filters operate at the macrozone level, with a common configuration for the North, Center and South macrozones and a distinct one for the Austral macrozone.

### 3.5.1 Asymmetric Temporal Filter

A pixel-level state-transition filter was applied to the gap-filled annual time series to reduce spurious interannual transitions. The filter applies asymmetric persistence criteria for glacier gain and loss, based on the assumption that glacier area loss may occur over shorter timescales than glacier area gain.

- A pixel transitions from non-glacier to glacier state only after gainK consecutive years of glacier classification (gainK = 5). This prevents seasonal snow from being misclassified as glacier gain.
- A pixel transitions from glacier to non-glacier state after lossM consecutive years of non-glacier classification (lossM = 2). The lower loss threshold reflects that genuine glacier retreat can occur over shorter periods.

To avoid the influence of the 1997–1998 El Niño event on the initial state estimation, the filter was initialized using the 1999 classification as an anchor year rather than computing a warmup majority from the earliest years of the series.

### 3.5.2 Spatial Elevation Constraint

The minimum glacier elevation for each hydrological basin was derived from the 2022 Public Glacier Inventory (IPG 2022) using the HMIN attribute. Pixels located more than 100 m below this basin-level minimum elevation threshold were removed. This constraint is based on the assumption that sustained glacier presence substantially below the minimum elevation reported in the inventory is unlikely under current climatic conditions. The 100 m offset was introduced to account for two sources of uncertainty: (1) possible differences between glacier margins at the beginning of the time series and the inventory reference period, given the documented recent retreat and mass loss of Andean glaciers; and (2) vertical uncertainty in the FABDEM digital elevation model in steep mountain terrain.

### 3.5.3 Minimum Persistence Rule (Rule C)

A minimum persistence filter was applied to macrozones 1–3 (North, Center, South) to remove pixels that were not classified as glacier for at least K_MIN = 5 consecutive years at any point in the 1998–2025 time series. This filter reduces residual false positives associated with persistent or recurrent snow patches that may remain after the temporal filtering steps. The filter was not applied to the Austral macrozone, where glacier margins may show genuine multi-year fluctuations that could be incorrectly removed by a minimum-persistence requirement.

The K_MIN = 5 threshold was selected as a conservative empirical parameter. It requires glacier occurrence to persist over multiple consecutive annual observations, thereby reducing short-lived snow signals while retaining pixels with sustained glacier-like temporal behavior. The threshold corresponds to approximately 18% of the 28-year time series and was used only in macrozones where transient snow contamination is more likely to affect isolated glacier detections.

## 3.6 Post-Classification Spatial Filters (Step 3)

Following temporal post-processing, three spatial filters were applied:

- **Minimum area filter**: glacier objects smaller than 0.01 km² were removed to eliminate small, isolated detections likely to be spurious. This threshold follows the minimum area adopted by the Randolph Glacier Inventory (RGI Consortium, 2017). A larger threshold of 0.02 km² was applied in the Austral macrozone, where glaciers are substantially larger and small isolated objects are more likely to represent classification noise than genuine ice bodies.

- **Chile´s boundary mask**: classifications were clipped to the national boundary to remove cross-border artefacts.

- **Small glacier rescue**: objects smaller than 0.01 km² intersecting glacieret polygons from the 2022 Public Glacier Inventory (IPG 2022) were reinstated to preserve small glacier bodies documented in the national inventory.

## 3.7 Special Development for the Austral Macrozone

The Austral macrozone required a methodological treatment distinct from that applied to the North, Center and South macrozones, owing to its particular climatic, geomorphological and image-availability conditions. This zone concentrates 88.93% of Chile's glacier area (DGA, 2022), which warrants a dedicated procedure to maximize classification quality under persistent cloud cover and complex glacier dynamics, including tidewater glaciers and advancing and retreating fronts.

### 3.7.1 Water-Frequency (FPOL) and Land-Cover (LULC) Correction

To correct the overextension of glacier tongues onto water bodies, a water-frequency measure — expressed as months per year with water (0–12) and derived from the MapBiomas Chile Water product — was used as an exclusion criterion. This measure, FPOL, is a polygon-averaged frequency: for each year, water-extent polygons were generated from the maximum water surface, and FPOL is the mean of the pixel frequencies falling within those polygons.

The correction was applied as an exclusion rule: any glacier pixel whose water frequency exceeds a monthly threshold is reclassified as water. A T−1 temporal offset was used, so that the classification of year T is corrected with the frequency of year T−1; because the annual mosaic is built from imagery of the first months of the year, the previous year's frequency provides the temporally consistent proxy.

Validation was carried out against photo-interpreted front polygons in eight cases (glacier × year), including both retreating and advancing glaciers. A threshold sweep was performed, comparing each candidate threshold against the uncorrected classification; a 7-month threshold was adopted as the production correction.

As a complement to the water-frequency filter, the land-cover (LULC) layer of Collection 2 was incorporated, using its water class (class 33) as an additional exclusion criterion, applied with the same exclusion logic — any glacier pixel coincident with the LULC water class is reclassified as water — and the same T−1 offset. The two layers are complementary: FPOL yields the maximum water extent and reaches the glacier fronts, whereas the LULC — built from annual-mean mosaics, and therefore carrying more seasonal snow and not fully reaching the fronts — provides a cleaner delineation of water bodies, removing icebergs and the interior of lakes and lagoons that the frequency filter does not necessarily reach.

Both filters were applied sequentially on the gap-fill output (FPOL with a 7-month threshold, followed by the LULC water class), together constituting the water correction of the glacier product.

### 3.7.2 Frequency-Based Persistence Filter

A temporal persistence filter was applied to correct sporadic omissions attributable to sensor noise or missing observations, without altering genuine glacier dynamics.

For each pixel, a frequency was computed as the number of years classified as glacier during the analysis period; years without data do not contribute to this count. Only pixels with a frequency of at least 17 years were treated as candidates for correction, on the assumption that high persistence indicates stable glacier presence and that intervening absences therefore most likely correspond to classification errors.

Filling was restricted to internal gaps, defined as glacier-free years between the first and last years in which the pixel was classified as glacier. This preserves both genuine onset (the real start of the series) and genuine disappearance (the real end), avoiding extrapolation of glacier presence beyond each pixel's observed activity interval. Operationally, the activity interval was delimited using cumulative operations on the chronologically ordered bands (progressive maximum forward and backward), whose intersection defines the internal years; internal gaps at candidate pixels were reclassified to the glacier class.

### 3.7.3 Asymmetric Temporal Filter

Unlike the North, Center and South macrozones — where the transition to glacier requires gainK = 5 years to prevent seasonal snow from being interpreted as glacier gain (Section 3.5.1) — the Austral macrozone adopts gainK = 3 and lossM = 2. The lower evidence requirement for gain reflects the glacier dynamics characteristic of Patagonia, where fronts undergo genuine multi-year advance and retreat cycles; a high gain threshold would remove real advances rather than filter noise. The same consideration underlies the exclusion of the minimum-persistence rule (Regla C) in this macrozone (Section 3.5.3). The filter's asymmetry allows sensitivity to glacier advance and retreat to be adjusted independently.

# 4 Validation Strategies

The glacier classification time series is validated against independent glacier outlines delineated by the Chilean Dirección General de Aguas (DGA) for selected glaciers at multiple dates. Validation is performed per glacier and year, and aggregated by glaciological macrozone and for the full validation set.

## 4.1 Reference Data

Reference outlines are drawn from two DGA technical documents: the Serie de Documentos Técnicos N°544 (Reporte de variaciones areales de glaciares relevantes monitoreados en el año 2025; SDT N°544, DGA, 2025), which provides recent glacier outlines, and the Serie de Informes Técnicos N°261 (Variaciones recientes de glaciares en Chile, según principales zonas glaciológicas; SIT N°261; DGA, 2011), which provides the earlier outlines. Together they supply DGA-delineated glacier polygons for a set of glaciers across several years, distributed over the four macrozones.

Because the product maps only bare (uncovered) ice, the validation set was restricted to glaciers whose surface was almost entirely exposed ice at the reference date. Glaciers with substantial debris cover or persistent seasonal snow were excluded, so that the reference polygon and the classified extent represent the same physical quantity and are directly comparable. The resulting set comprises 47 glacier–year outlines (10 North, 12 Center, 17 South, 8 Austral).

## 4.2 Validation Metric – Jaccard Index

Agreement between each classified glacier extent and its corresponding DGA reference polygon is quantified with the Jaccard index (J), also known as Intersection over Union:

$$J = \frac{|A \cap B|}{|A \cup B|}$$

Where:

A = classified glacier area

B = DGA reference polygon for the same glacier and year.

J ranges from 0 (no spatial overlap) to 1 (perfect coincidence). Unlike a comparison of total areas, the Jaccard index penalizes both omission (reference ice not classified) and commission (classified ice outside the reference), and is sensitive to the spatial coincidence of the two extents rather than only their aggregate size.

## 4.3 Reporting

Jaccard values are reported for each glacier and year (Table 4.1), with a mean per macrozone and a global mean across all validation samples, presented separately by macrozone to reflect the distinct classification challenges of each zone: commission from seasonal snow in North and Center, mixed pixels at glacier margins in South, and calving-front dynamics in Austral.

*Table 4.1. Jaccard index (J) between classified glacier extent and DGA reference polygons, by glacier, year and macrozone. Per-macrozone and global means are reported; the J column is to be completed with the computed values.*

| Glacier | Year | Source | J |
|---|---|---|---|
| **Macrozone Norte** | | | |
| Llullaillaco | 2001 | SIT N°261 | 0.72 |
| Llullaillaco | 2006 | SIT N°261 | 0.84 |
| Llullaillaco | 2016 | SDT N°544 | 0.84 |
| Llullaillaco | 2020 | SDT N°544 | 0.86 |
| Llullaillaco | 2024 | SDT N°544 | 0.94 |
| Llullaillaco | 2025 | SDT N°544 | 0.93 |
| Nevado Tres Cruces | 2025 | SDT N°544 | 0.94 |
| Sillajhuay | 2008 | SIT N°261 | 0.31 |
| Sillajhuay | 2025 | SDT N°544 | 0.68 |
| Tronquitos | 2025 | SDT N°544 | 0.98 |
| **Macrozone Norte — mean (n=10)** | | | **0.80** |
| **Macrozone Centro** | | | |
| Azufre | 2001 | SIT N°261 | 0.75 |
| Azufre | 2006 | SIT N°261 | 0.89 |
| Azufre | 2015 | SDT N°544 | 0.91 |
| Azufre | 2019 | SDT N°544 | 0.92 |
| Azufre | 2023 | SDT N°544 | 0.74 |
| Azufre | 2024 | SDT N°544 | 0.74 |
| Azufre | 2025 | SDT N°544 | 0.74 |
| Olivares Gamma | 2019 | SDT N°544 | 0.93 |
| Olivares Gamma | 2022 | SDT N°544 | 0.94 |
| Olivares Gamma | 2023 | SDT N°544 | 0.92 |
| Olivares Gamma | 2024 | SDT N°544 | 0.90 |
| Olivares Gamma | 2025 | SDT N°544 | 0.93 |
| **Macrozone Centro — mean (n=12)** | | | **0.86** |
| **Macrozone Sur** | | | |
| Antuco | 2011 | SIT N°261 | 0.98 |
| Callaqui | 2011 | SIT N°261 | 0.93 |
| Llaima | 2011 | SIT N°261 | 0.29 |
| Lonquimay | 2010 | SIT N°261 | 0.32 |
| Michinmahuida | 2025 | SDT N°544 | 0.98 |
| Mocho-Choshuenco | 2025 | SDT N°544 | 0.95 |
| Nevados de Chillán | 2011 | SIT N°261 | 0.88 |
| Osorno | 2011 | SIT N°261 | 0.93 |
| Puntiagudo | 2005 | SIT N°261 | 0.58 |
| Puyehue | 2011 | SIT N°261 | 0.77 |
| Queulat | 2025 | SDT N°544 | 0.91 |
| Sierra Nevada | 2011 | SIT N°261 | 0.96 |
| Sierra Velluda | 2011 | SIT N°261 | 0.73 |
| Sierra Velluda | 2025 | SDT N°544 | 0.72 |
| Sollipulli | 2011 | SIT N°261 | 0.98 |
| Tolhuaca | 2011 | SIT N°261 | 0.71 |
| Yanteles | 2025 | SDT N°544 | 0.97 |
| **Macrozone Sur — mean (n=17)** | | | **0.80** |
| **Macrozone Austral** | | | |
| Greve | 2000 | SIT N°261 | 0.92 |
| Greve | 2006 | SIT N°261 | 0.91 |
| Greve | 2009 | SIT N°261 | 0.82 |
| Jorge Montt | 2003 | SIT N°261 | 0.98 |
| Jorge Montt | 2009 | SIT N°261 | 0.89 |
| Nef | 2000 | SIT N°261 | 0.56 |
| Nef | 2017 | SDT N°544 | 0.33 |
| Pío XI | 2019 | SDT N°544 | 0.95 |
| **Macrozone Austral — mean (n=8)** | | | **0.80** |
| **Global mean (n=47)** | | | **0.81** |

### 4.4 Limitations

Several factors constrain the accuracy assessment and the product itself:

- **Reduced image availability in the early years**. For the earliest part of the series (approximately 1998–2005), fewer cloud- and snow-free scenes are available to build the annual composites. This lowers the likelihood of capturing true end-of-summer minimum-snow conditions, so residual seasonal snow may be retained and classified as glacier, potentially producing a slight overestimation of glacier area in those years.

- **Exclusion of debris-covered ice and rock glaciers**. The product maps bare (uncovered) ice only. Debris-covered glacier tongues and rock glaciers are spectrally similar to the surrounding terrain and cannot be reliably separated using optical imagery and a machine learning classifier trained on exposed ice; they are therefore not included. Consequently, the mapped extent represents bare-ice area and is not directly comparable to inventories that incorporate debris-covered or rock-glacier classes.

- **Discontinuous validation data**. DGA reference outlines are available only for specific glaciers at specific years, so not every year of the 1998–2025 series can be independently validated. Accuracy in unvalidated years — including parts of the interval of most rapid change — is inferred from the temporally bracketing reference samples rather than measured directly.

- **Tephra-covered glaciers on active volcanoes.** A small number of validation targets are glaciers on active volcanoes (e.g., Llaima, Lonquimay, Puntiagudo) whose surfaces carry tephra and ash. These are inherently difficult to delineate from optical imagery and show lower agreement (Jaccard) than clean-ice targets. They are retained in the validation set for transparency, but their lower scores reflect the difficulty of the surface rather than a systematic failure of the method, and they contribute minimally to total glacier area.

- **Spatial resolution (30 m).** Near the pixel scale, small ice bodies and glacierets — common in the North Macrozone — carry a larger relative area uncertainty due to mixed pixels at their margins.

- **Multi-sensor consistency**. The series combines Landsat 5, 7, 8 and 9 with Sentinel-2. The Landsat 7 SLC-off gaps (from 2003) and the Landsat-to-Sentinel-2 transition in the southern zone can introduce minor artefacts or step changes along the time series, which post-processing mitigates but does not fully eliminate.

## 5 Concluding Remarks and Perspectives

The MapBiomas Agua Chile glacier product provides, for the first time, a consistent annual record of bare-ice glacier extent across the full Chilean territory from 1998 to 2025. The resulting time series captures the broad pattern of glacier retreat documented across the Chilean Andes while limiting artefacts from seasonal snow and interannual climate variability.

Future versions of this collection will aim to: map debris-covered glaciers; classify rock glaciers using deep-learning methods; integrate SAR observations to improve coverage in the persistently cloud-covered Austral zone; and harmonize the Landsat–Sentinel-2 transition to reduce potential systematic biases after 2017.

# 6 References

Dirección General de Aguas (DGA). (2011). Variaciones recientes de glaciares en Chile, según principales zonas glaciológicas (SIT N°261). Ministerio de Obras Públicas, Chile. (Realizado por el Centro de Estudios Científicos, CECs.)

Dirección General de Aguas (DGA). (2022). Inventario Público de Glaciares 2022 (IPG2022_v1). Ministerio de Obras Públicas, Chile.

Dirección General de Aguas (DGA). (2025). Reporte de variaciones areales de glaciares relevantes monitoreados en el año 2025 (SDT N°544). Ministerio de Obras Públicas, Chile.

Dussaillant, I., Berthier, E., Brun, F., Masiokas, M., Hugonnet, R., Favier, V., Rabatel, A., Pitte, P. & Ruiz, L. (2019). Two decades of glacier mass loss along the Andes. Nature Geoscience, 12, 802–808. https://doi.org/10.1038/s41561-019-0432-5

Gorelick, N., Hancher, M., Dixon, M., Ilyushchenko, S., Thau, D. & Moore, R. (2017). Google Earth Engine: Planetary-scale geospatial analysis for everyone. Remote Sensing of Environment, 202, 18–27.

Mohammadi, B., Pilesjö, P. & Duan, Z. (2023). The superiority of the Adjusted Normalized Difference Snow Index (ANDSI) for mapping glaciers using Sentinel-2 multispectral satellite imagery. GIScience & Remote Sensing, 60(1), 2257978. https://doi.org/10.1080/15481603.2023.2257978

Pasquarella, V. J., Brown, C. F., Czerwinski, W. & Rucklidge, W. J. (2023). Comprehensive quality assessment of optical satellite imagery using weakly supervised video learning. Proceedings of the IEEE/CVF Conference on Computer Vision and Pattern Recognition (CVPR) Workshops, 2124–2134.

RGI Consortium. (2017). Randolph Glacier Inventory – A Dataset of Global Glacier Outlines, Version 6.0. Global Land Ice Measurements from Space (GLIMS), Boulder, Colorado, USA. https://doi.org/10.7265/N5-RGI-60

Saavedra, F., Hernández-Duarte, A., Caro, A., Rabatel, A., Fassnacht, S., Condom, T., Kampf, S., Masiokas, M., Romero, C., Aguirre, Y., González, D., Contreras, V., Medina, J. & Arancibia, P. (2026). Spatial and temporal variability of snow in the Andes using MODIS snow product 2000–2025. Frontiers in Earth Science, 14, 1564035. https://doi.org/10.3389/feart.2026.1564035